Title
An Effective Fractal-Tree Closure Model for Simulating Blood Flow in Large Arterial Networks

Journal
Annals of Biomedical Engineering, 43(6)

ISSN
0145-3068

Authors
Perdikaris, Paris
Grinberg, Leopold
Karniadakis, George Em

Publication Date
2015-06-01

DOI
10.1007/s10439-014-1221-3

Peer reviewed

Published in final edited form as:

Ann Biomed Eng. 2015 June ; 43(6): 1432–1442. doi:10.1007/s10439-014-1221-3.

An efective fractal-tree closure model for simulating blood flow in large arterial networks

Paris Perdikaris[*,1], **Leopold Grinberg**[†,2], and **George Em. Karniadakis**[‡,1]

[1]Division of Applied Mathematics, Brown University, Providence RI, USA

[2]IBM T. J. Watson Research Center, Cambdridge MA, USA

Abstract

The aim of the present work is to address the closure problem for hemodynamic simulations by developing a exible and effective model that accurately distributes flow in the downstream vasculature and can stably provide a physiological pressure out flow boundary condition. To achieve this goal, we model blood flow in the sub-pixel vasculature by using a non-linear 1D model in self-similar networks of compliant arteries that mimic the structure and hierarchy of vessels in the meso-vascular regime (radii 500 μm – 10 μm). We introduce a variable vessel length-to-radius ratio for small arteries and arterioles, while also addressing non-Newtonian blood rheology and arterial wall viscoelasticity effects in small arteries and arterioles. This methodology aims to overcome substantial cut-off radius sensitivities, typically arising in structured tree and linearized impedance models. The proposed model is not sensitive to out flow boundary conditions applied at the end points of the fractal network, and thus does not require calibration of resistance/capacitance parameters typically required for out flow conditions.

The proposed model convergences to a periodic state in two cardiac cycles even when started from zero-flow initial conditions. The resulting fractal-trees typically consist of thousands to millions of arteries, posing the need for efficient parallel algorithms. To this end, we have scaled up a Discontinuous Galerkin solver that utilizes the MPI/OpenMP hybrid programming paradigm to thousands of computer cores, and can simulate blood flow in networks of millions of arterial segments at the rate of one cycle per 5 minutes. The proposed model has been extensively tested on a large and complex cranial network with 50 parent, patient-specific arteries and 21 outlets to which fractal trees where attached, resulting to a network of up to 4,392,484 vessels in total, and a detailed network of the arm with 276 parent arteries and 103 outlets (a total of 702,188 vessels after attaching the fractal trees), returning physiological flow and pressure wave predictions without requiring any parameter estimation or calibration procedures.

We present a novel methodology to overcome substantial cut-off radius sensitivities

Keywords

computational hemodynamics; 1D blood flow; outflow boundary conditions; fractal arterial networks; fractional modeling; high performance computing; Circle of Willis; arm network

[*]paris_perdikaris@brown.edu. [†]leopoldgrinberg@us.ibm.com. [‡]george_karniadakis@brown.edu.

1 Introduction

The field of computational hemodynamics has undergone great growth in the last 20 years, producing more reliable mathematical models, utilizing modern computer architectures for parallel simulations, and allowing for high delity simulations in computational domains reconstructed from patient-specific medical imaging data [28, 12, 23]. While simulations have significantly pushed the boundaries of problem size, performing full scale blood flow simulations on the human arterial network remains intractable hence the need for formulating a proper closure problem for simulations in truncated domains. It is a common practice to reconstruct blood vessel network from medical images covering a particular region, where the resulting models capture only relatively large vessels and additional modeling is required to account for hemodynamics in the truncated vasculature. specifically, in this article we focus on modeling out flow boundary conditions for simulations in arterial networks with multiple outlets.

Generally speaking, there are two options to properly truncate the computational domain a) use flowrate and/or pressure measurements to directly impose patient-specific data at the outlets, i.e., avoid modeling the truncated arterial tree; and b) use low-dimensional models to *simulate* the flow in the truncated domain. Clearly, in the absence of clinically measured data one has to resort to modeling. Ideally, closure models should be based on sound assumptions with respect to the physics of the problem, be as free as possible of parametric sensitivities, and be fast to solve. In the following we review the current closure models and point to their advantages and limitations.

The widely used simplest representation of the sub-pixel vasculature comes from zero-dimensional (0D) lumped parameter models. This approach consists of additive combinations of electrical elements, such as resistors R, capacitors C and inductors L, that aim to capture the effective resistance and compliance effects of the neglected arterial networks [1, 23]. The main advantage of this approach is its implementation simplicity and low computational cost, as it only requires the solution of a linear ordinary differential equation at each terminal outlet. The key disadvantage of this method is the inherent difficulty in estimating the 0D model parameters in absence of local flow measurements at the outlets, in combination with the high sensitivity of the flow model output on these parameters. Recent studies have proposed iterative calibration procedures, in which the problem is solved multiple times until a set of parameters that yields a physiological solution is identified [2, 18, 15]. Despite their evident limitations, 0D models have been extensively used in the literature [23, 1, 13, 2, 27], and results for accurately calibrated models have been successfully validated against *in-vivo* measurements [23]. However, it seems that the obtained windkessel model parameters are not uniform for each arterial network and a calibration procedure has to be repeated to accommodate any network modifications.

An alternative closure model, first put forth by Olufsen et. al. [19], considers modeling the downstream vasculature as a self-similar network of compliant arteries in which a linearized one-dimensional (1D) model is used to estimate the pressure out flow boundary condition as a function of the flowrate time history. The structure of the fractal arterial trees is motivated by the findings of Zamir et. al. [29], while the elasticity parameters vary with the vessel's

radius by tting experimental measurements. The resulting out flow boundary condition is obtained by computing a convolution operator that relates pressure to flow time history at each of the outlets. Although this approach offers a more detailed representation of the downstream dynamics, it is known to be highly sensitive to the cut-off radius of the structured tree [5], suggesting the need for a calibration procedure. Some other limitations of this method include the high number of simulation cycles required to reach a periodic flow state, the costly computation of the convolutions in every time-step, as well as the neglect of the Fahraeus-Lindqvist effect in small arteries and arterioles [21] , and the viscoelastic response of the arterial wall. Recent advances have extended the use of the structured tree model to unsteady problems and explored the use of the Laplace transform to speed up the convergence to a periodic flow state [6].

In the case where flow measurements at the outlets are present, Grinberg and Karniadakis [13] have proposed a simple way of constructing a two-element 0D model that is able to reproduce the measured data *in-silico*. According to [13], the time varying resistance parameters are derived from the measured flowrates, hence no calibration of the 0D model is required, and simulating 5-10% of a cardiac cycle is sufficient for the mass flow distribution to converge to the reference data.

In this work our main goal is to construct a robust model that eliminates parametric sensitivities and is able to provide a physiological closure to patient-specific hemodynamics simulations with a large number of outlets. We simulate the truncated network by constructing fractal networks of small arteries and arterioles with radii in the range ($10 – 500\ \mu m$) that bridge the gap between the outlets of a patient-specific domain and the capillary bed. We simulate hemodynamics using a fully nonlinear 1D solver that accounts for non-Newtonian flow effects and wall viscoelasticity. As this task requires us to resolve flow in networks of thousands to millions of arteries, we have scaled up a parallel 1D Discontinuous Galerkin solver to modern multi-core architectures, moving closer towards the capability of producing *near real-time* numerical solutions.

In section 2 we outline the nonlinear 1D closure model and highlight key implementation aspects. Section 3 elaborates on the simulation setup, the test cases considered and the main findings of this study. In particular, we address the flow sensitivity issue on the terminal cut-off radius and propose a way to eliminate it by introducing an ansatz on the vessel's length-to-radius ratio for small arterioles. Moreover, we study how the predicted hemodynamics is affected by the Fahraeus-Lindqvist effect [21] in small arteries and arterioles, and by different choices of boundary conditions at the very distal outlets of the fractal domains. Finally, section 4 summarizes our key findings and provides motivation on possible future thrusts of research.

2 Methods

2.1 The 1D model

We consider viscous incompressible 1D flow in a compliant tube. The flow dynamics is governed by a nonlinear hyperbolic system of partial differential equations that can be directly derived from the Navier-Stokes equations under the assumptions of axial symmetry,

dominance of the axial velocity component, radial displacements of the arterial wall, and constant internal pressure on each cross section [9].

The conservation of mass and momentum can be formulated in space-time (*A; U*) variables as (see [24] for a detailed derivation) :

$$\begin{cases} \frac{\partial A}{\partial t}+\frac{\partial (AU)}{\partial x}=0 \\ \frac{\partial U}{\partial t}+U\partial U\partial x=-\frac{1}{\rho}\frac{\partial p}{\partial x}+K_r\frac{U}{\rho A}, \end{cases} \quad (1)$$

where *x* is the axial coordinate across the vessel's length, *t* is time, *A*(*x; t*) is the cross-sectional area of the lumen, *U*(*x; t*) is average axial uid velocity, *Q*(*x; t*) = *AU* is the mass flux, *p*(*x; t*) is the internal pressure averaged over the tube's cross-section, and K_r is a friction parameter that depends on the velocity profile chosen [24]. Here we use an axisymmetric fluid velocity *u*(*x; r; t*) profile that satisfies the no-slip condition.

$$u\left(x,r,t\right)=U\frac{\zeta+2}{\zeta}\left\{1-\left(\frac{r}{R}\right)^{\zeta}\right\}, \quad (2)$$

with *R*(*x; t*) being the lumen radius, a constant, and *r* the radial coordinate. Following [9], ζ = 9 gives a good t to experimental blood flow data and ζ = 2 returns the parabolic flow profile. Moreover, $U=\frac{1}{R^2}\int_0^R 2rudr$, and the friction parameter can be expressed as $K_r=\frac{2v}{U}\frac{A}{R}\left[\frac{\partial u}{\pi r}\right]_R=-22\mu\pi$ (see [24]), with *μ* being the blood viscosity that is a function of the lumen radius and the blood hematocrit, based on the findings of Pries et. al. [21].

System (1) can be solved for (*A; U*) after introducing a constitutive law for the arterial wall that relates the cross sectional area *A* to pressure *p*. The theory of quasi-linear viscoelasticity [10] provides a framework under which general soft tissue constitutive laws can be formulated as additive combinations of simple elastic and viscous elements. Based on this approach we can derive a pressure-area relation of the form [20]:

$$p\left(x,t\right)=\int_0^t G\left(t-\gamma\right)\frac{\partial p^e\left(x,y\right)}{\partial\gamma}d\gamma, \quad (3)$$

where *G*(*t*) is a stress relaxation kernel and p^e(*x; t*) is the static elastic response of the tissue derived directly from the Laplace tube law [20]:

$$p^e=p_{ext}+\frac{\sqrt{\pi}Eh}{\left(1-\nu^2\right)\sqrt{A_0}\sqrt{A}}\left(\sqrt{A}-\sqrt{A_0}\right) \quad (4)$$

Here, p_{ext} is the external pressure on the arterial wall, *E* is the Young modulus of the wall, *h* is the wall thickness, and is the Poisson ratio.

The convolution integral in Eq. 3 introduces a dependence on the cross sectional area time history, with the tissue model being determined by the choice of the stress relaxation kernel *G*(*t*). Typically, one introduces a parametric representation of *G*(*t*) that fits given

experimental measurements. In this work we have considered a stress relaxation function derived from a fractional-order Standard Linear Solid model [20]:

$$G(t) = E\left(\frac{\tau_\epsilon}{\tau_\sigma}\right)^\alpha + E\left(\left[\frac{\tau_\epsilon}{\tau_\sigma}\right]^\alpha - 1\right) E_{\alpha,1}\left(-\left[\frac{t}{\tau_\sigma}\right]^\alpha\right), \quad (5)$$

parametrized by the Young modulus *E*, the fractional order , and the viscoelastic relaxation times $\{\tau\varepsilon, \tau\delta\}$, while $_{Ea,\beta}$ (*t*) is a two parameter Mittag-Leffer function [16]. Arterial wall constitutive laws based on fractional calculus have been shown to provide a good fit to *in-vivo* stress relaxation data [8, 7], accounting for a continuum relaxation spectrum and exhibiting lower sensitivity on input parameters compared to integer-order models [8, 20]. The fractional order $\alpha \in [0, 1]$ controls the interplay between elastic energy storage and viscoelastic dissipation and its effect on hemodynamics is manifested by modulation of the propagating pressure waveform [20]. This wall model is able to capture the effects of viscoelastic hysteresis, creep and stress relaxation, although it does not account for non-linear tissue stiffening under high stress.

The system of equations in Eq. 1 can be recast in a conservative form as [24]:

$$\frac{\partial \mathbf{U}}{\partial t} + \frac{\partial \mathbf{F}(\mathbf{U})}{\partial x} = \mathbf{S}(\mathbf{U}), \quad \mathbf{U} = \begin{bmatrix} A \\ U \end{bmatrix}, \quad \mathbf{F} = \begin{bmatrix} AU \\ \frac{U^2}{2} + \frac{p^e}{\rho} \end{bmatrix} + \begin{bmatrix} 0 \\ \frac{p^v}{\rho} \end{bmatrix}, \quad \mathbf{S}(\mathbf{U}) = \begin{bmatrix} 0 \\ -22\mu\pi\frac{U}{\rho A} \end{bmatrix}, \quad (6)$$

where the viscoelastic component of the total pressure $p^v(x; t)$ can be derived using Eqs.(3,5) as [20]:

$$p^v(x,t) = \frac{1}{\tau_\sigma}\left(1 - \left[\frac{\tau_\epsilon}{\tau_\sigma}\right]^\alpha\right) \int_0^t E_{\alpha,0}\left(-\left[\frac{t-\gamma}{\tau_\sigma}\right]^\alpha\right) p^e(\gamma)\, d\gamma \quad (7)$$

For the numerical solution of the above system we have adopted the Discontinuous Galerkin scheme first put forth by [24]. Spatial discretization consists of dividing each arterial domain Ω into *Nel* elemental non-overlapping regions. A continuous solution within each element is retrieved as a linear combination of orthogonal Legendre polynomials, while discontinuities may appear across elemental interfaces. Global continuity is restored by flux upwinding across elemental interfaces, bifurcations and junctions, with conservation of mass, continuity of Riemann invariants and continuity of the total pressure being ensured by the solution of a Riemann problem [24]. Finally, time integration is performed explicitly using a second-order accurate Adams-Bashforth scheme.

2.2 Fractal-tree closure model

Here we build upon the structured tree framework first put forth by Olufsen et. al. [19] and model downstream flow dynamics by structured trees that aim to bridge the geometric scale gap between outlets with diameters of $\mathcal{O}(cm)$ and the small arterioles that enter the capillary network $\mathcal{O}(\mu m)$. This approach is motivated by the findings of Zamir et. al. [29] and Cassot et. al. [3], which indicate that branching patterns of arteries in the meso-vascular regime resemble fractal laws as follows. A parent vessel of radius r_0 bifurcates into two daughter vessels with $r_1 = \delta r_0$; $r_2 = \beta_0$, where

$$\delta=\left(1+\gamma^{z/2}\right)^{-1/z}, \quad \beta=\delta\sqrt{\gamma}, \quad \gamma=\left(\frac{r_2}{r_1}\right)^2, \quad r_2 \leq r_1 \quad (8)$$

Starting from an outlet with radius r_0, the resulting fractal-tree is uniquely determined by the parametric set of $\{r_{cut}, L/r, \delta, \beta, \gamma, z\}$, where L/r is the length over radius ratio of each vessel and r_{cut} is the terminal cut-off radius of the tree (see Figure 2), β, δ are the parent-daughter radius ratios, quantifies the asymmetry of the network, and z is a power law exponent that describes the fluid flow distribution from parent to daughter vessels at each bifurcation [29, 3]. Of these parameters, only r_{cut} may be considered as user input, while the rest may be estimated from medical imaging either in a patient-specific setting or based on population samples. Although δ, β, γ and z seem to be independent of location in the arterial tree [26, 29, 3], the length to radius ratio L/r exhibits a local character, varying significantly among different organs and typically taking values within the range L/r = 10 60 [29]. The choice of these parameters determines the size of the generated fractal-tree, and, therefore, the total downstream resistance experienced by each outlet.

The elastic property of the arterial wall is estimated using the experimental fit put forth by Olufsen *et. al*. [19] that relates the Young's modulus times the thickness of the arterial wall with the vessel radius (see Fig. 3 in [19]). This is the exact relation that has been employed in our work for $r > 500$ μm, where the curve gives a good fit to the observed experimental data. However, for $r < 500$ μm the exponential fit becomes singular as the vessel radius approaches 0. This singularity results to unrealistic predictions, as it implies that small arteries become exponentially stiffer with decreasing radius. To overcome this limitation, we have assumed that vessels with $r <= 500$ μm have the same elastic modulus, set to the value predicted by Olufsen's law for $r = 500$ μm, corresponding to a threshold value of $Eh/r_0 = 7.35 \cdot 10^6 g/sec^2/cm$. Although this choice is arbitrary, we believe it is realistic as small arteries and arterioles are not known to exhibit mechanical responses that may differ by up to 2 orders of magnitude, as predicted from Olufsen's t for $r << 500$ μm.

2.3 Implementation aspects

In this work we model flow dynamics in the fractal network using the non-linear conservation law in Eq. 1. This allows us to simulate unsteady blood flow in arterial networks spanning multiple spatial scales, to naturally account for the vascular resistance of the arteriolar regime, as well as to resolve the systemic pressure drop, most of which is known to occur at the level of arterioles [17]. Moreover, we are able to consider important non-Newtonian flow effects in small arteries and arterioles, as well as to include the effects of wall viscoelasticity. From the implementation perspective, this approach introduces a computational challenge as the resulting arterial network may consist of millions of degrees of freedom, mandating the need for efficient numerical methods and algorithms.

As the cut-off radius is decreased networks consisting of millions of arteries are generated, rendering simulation a non-trivial task. Here, we address this computational challenge by developing a parallel solver based on hybrid programming paradigm that utilizes the MPI and OpenMP libraries, allowing us to decompose the problem among multiple compute nodes as well as explore intra-node parallelism via multithreading. This approach allowed us

to scale up our 1D blood flow solver on the IBM Blue Gene/Q architecture and integrate Eq. 1 at the rate of 10^{-8} *s* per vessel, per time-step. Based on our experience in simulating 1D flow in networks of thousands to millions arteries, about 100-150 of modern CPUs are adequate for simulating one cardiac cycle in about five minutes. We also envision that further reduction in required CPU time is possible by performing code optimization and scaling to larger number of CPUs.

2.4 Case studies and simulation setup

Flow in the Circle of Willis (CoW)—For our first test case we consider a large patient-specific network consisting of the 50 largest arteries in the human brain, see Fig. 2. The data was obtained at the Department of Neurosurgery at Children's Hospital, Boston MA, USA. First, the 3D geometry was reconstructed from high-resolution magnetic resonance images (MRI) using an “in house” developed software package, and then, the 1D domain was extracted from the centerlines of the 3D vasculature. Consequently, the 1D representation preserves the mean diameter and length of each of the 3D segments, while omitting curvature as well as bifurcation and junction branching angle information. The exact dimensions and elasticity parameters of each arterial segment, as well as details of the reconstruction process are given in [11]. The nonlinear 1D blood flow system (Eq. 1) is solved in the patient-specific parent network (50 cranial arteries) and the fractal trees attached to each one of the 21 outlets.

The network has 4 inlets (see Fig. 2): the two internal carotid (ICA) and two vertebral (VA) arteries, where we apply accurate PC-MRI flowrate measurements [11]. To ensure stability we have chosen a very small time-step $\Delta t = 10^{-6}$ *s* due to the high polynomial order (ranging between 3-7 depending on the vessel's length) and the viscoelastic dissipation introduced by the arterial wall response modeled using Eq. 7 with $\alpha = 1$ (integer-order Standard Linear Solid model). The elasticity parameters are taken from [11], the viscoelastic relaxation times where set to $\tau_\varepsilon = 0.050s$ and $\tau_\delta = 0.025s$ [20], and the external pressure p_{ext} was taken equal to 15mmHg, corresponding to the mean pressure of the cerebrospinal fluid [23].

Flow in a detailed network of the arm—For our second test case we consider a detailed arterial representation of the arm based on the work of Watanabe et. al. [27]. This network consists of 246 arteries with 105 terminal outlets, 124 bifurcation points, 18 merging junctions and 85 perforator vessels [27] (see Fig. 3). Each arterial segment is discretized in space using 1 DG element per centimeter of vessel's length and a polynomial approximation of second order, while the time-step was taken equal to $\Delta t = 10^{-5}$ *s*. Following Watanabe et. al. we have employed a purely elastic constitutive law parametrized by the data reported in [27]. Flow is driven by imposing a physiological flowrate waveform at the inlet of the axillary artery based on information available in the medical literature [27]. Similarly, the 1D flow equations (Eq. 1) are solved treating the parent arm network (276 arteries) and the fractal trees attached to each one of the 103 outlets, as a whole.

In both the arm and cranial cases we have imposed absorbing wave out flow boundary conditions at all distal outlets of the fractal-trees by setting the corresponding Riemann invariant to zero. Blood viscosity is variable in space with the vessel's radius according to

the experimental ts of Pries et. al. [21], while the blood hematocrit is considered constant and equal to 0.45. The initial conditions are $(A;\ U;\ p)_{t=0} = (A_0;\ 0;\ p_{ext})$, and discretization parameters are chosen such that the computed solution does not depend on further resolution re nement.

Starting from each outlet of the of the parent CoW or arm network and given a user specified cut-off radius, we construct several generations of *asymmetrically* bifurcating fractal-trees. The trees are parametrized by $\{r_{cut},\ _{L/r} = 50,\ \delta = 0.9,\ \beta = 0.6,\ \gamma = 0.41,\ z = 2.76\}$, following the values suggested by Zamir et. al. [29]. In Table 1 we report the size of the resulting arterial network as well as the average number of generations attached to the parent domain for both the CoW and arm cases.

3 Results

In this section we present the main findings of our study. First, we demonstrate the well known issue of sensitivity on the cut-off radius of the fractal-trees [5], and propose an effective way of eliminating it by introducing an ansatz for selecting the length-to-radius ratio of the generated small arteries and arterioles. Second, we study two different blood rheology models in order to address the Fahraeus-Lindqvist effect [21] in small arteries and arterioles and quantify its effect on hemodynamics. Last, we present results on the effect of imposing different types of out flow boundary conditions at the distal outlets of fractal-trees.

3.1 Model sensitivity on the cut-off radius

Results of the first set of simulations with xed *L/r* ratio are shown in Figure 4, The numerical solution is obtained using fractal-trees parametrized by the values suggested in [29]. Pressure and flow rate waves are probed at the midpoint of the basilar (CoW case) and radial (arm case) arteries, respectively, demonstrating the high sensitivity on the choice of the cut-off radius. In particular, although the model predicts a consistent flow distribution and pressure drop across the arterial network, the computed pressure wave has a non-physiological magnitude, with the systolic pressure exceeding 200mmHg as the cut-off radius is decreased. This observation is in agreement with the results reported by Olufsen et el [19], Steele et. al. [25], and Cousins et. al. [5, 6], highlighting the main drawback of structured tree-type out flow boundary conditions. A justification of this inconsistency can be given based on the fact that as we decrease the cut-off radius, we greatly increase the size of the generated fractal-trees, leading to a potential overestimation of the total downstream resistance experienced by the outlets of the parent network.

3.2 Overcoming the cut-off radius sensitivity

One possible solution is to terminate the fractal-tree once the total volume of the generated network reaches a target value that is based on measuring (or estimating) the arterial fraction of the total blood volume considered. This approach can be applied for the CoW case as follows. First, we assume an estimate for the cerebral blood volume of about 120mL [22]. Then, following the findings of Ito *et. al*. [14], we take the true arterial fraction of the cerebral blood volume to be about 30%. Using this estimate we can compute the target arterial volume as $120\ 30\% \approx 35mL$. The main drawback of this approach is that it lacks

generality as the suggested termination criterion is only applicable for cases where an estimate of the blood volume and its corresponding arterial fraction at the region of interest is known.

Another possible solution is to adopt a tiered approach for selecting the parameters that govern the structure of fractal-trees, allowing $\{L/r, \delta, \beta, \gamma, z\}$ to vary with the vessel's radius based on experimental data [26]. This approach was successfully employed by Steele et. al. [25] and Cousins [5, 6, 4], although it was reported to be case dependent, potentially leading to inconsistencies if no model calibration is performed [4]. While our own experience confirms these findings, here we focus our study on testing an alternative way of selecting the length to radius ratio L/r that can effectively eliminate the sensitivity on the cut-off radius and produce physiologically correct results for patient-specific networks without the need of model calibration. To this end, we consider $\{\delta, \beta, \gamma, z\}$ to be constant across the tree, while introducing the ansatz that the L/r ratio is a linearly decreasing function once the radius becomes smaller than a given threshold r^* (see Figure 5).

In Figure 6 we present simulation results where the fractal-trees were generated using the proposed ansatz for the L/r ratio and no prior model calibration was performed. The solution is probed at the same spatial locations, namely the midpoint of the basilar (CoW case) and radial (arm case) arteries, respectively. For the CoW case, we have chosen a threshold of $r^* = 150\ \mu m$, as this value generates a network that matches the target volume of $35mL$ for a cut-off radius $r_{cut} = 30\ \mu m$ (see Figure 5). We observe that as the cut-off radius is decreased, the propagated flow and pressure waves converge to a physiologically correct plateau. This convergence is best quantified by computing the relative error of the pressure wave between cases with different cutoff radii and a reference case (see table inscribed in Figure 6). We also confirm that these results can be also reproduced if we assumed a constant L/r ratio and terminated the fractal-trees once the target volume of $35mL$ is reached ($r_{cut} = 60\ \mu m$, see Figure 5).

For the arm case, there does not exist (to our knowledge) an estimate for neither the blood volume nor for the arterial fraction of the blood volume. Hence, for this case, no estimate for the target volume can be computed, and r^* needs to be tuned by the user in order for the model to return physiologically correct results. Moreover, pressure wave propagation is expected to be sensitive to the choice of r^*, hence a calibration procedures is needed to obtain physiologically sound results. Although this is a limitation of the proposed framework, we believe that it is not a major one as only a single parameter, r^*, needs to be calibrated. On the contrary, if one wishes to employ the most widely used lumped closure model, the 3-element windkessel, immediately faces the problem of calibrating 206 resistance and capacitance parameters (the parent network consists of 276 arteries and 103 outlets) [27, 23, 28]. Consequently, here we have chosen a L/r relation with a threshold radius of $r^* = 500\ \mu m$ (see Figure 5). Similarly, the flowrate and pressure waves converge to a plateau solution that is no longer sensitive on further decreasing the cut-off radius r_{cut} (see Figure 6). Here, although the predicted waveforms are able to reproduce a physiological flow distribution, pressure drop and key wave propagation features such as the dicrotic and the anacrotic notch (see Figure 7), the computed pressure exceeds the physiologically correct range. This is because the arm network (courtesy of Pablo J. Blanco, LLNC [27]) is

not patient-specific but has been meticulously constructed from anatomical references available in the medical community, and our choice of $r^* = 500\ \mu m$ was an approximation. specifically, this network is missing several outlets that need to be considered if we hope to compute a physiologically correct pressure wave without the need of several iterations of a model calibration procedure.

3.3 The Fahraeus-Lindqvist effect

In order to accurately model blood flow in small arteries and arterioles ($50\ \mu m \leq r\ 500\ \mu m$), one needs to take into account the dependence of the apparent blood viscosity on the hematocrit and the vessel's radius (the Fahraeus-Lindqvist effect [21]). Here, we have performed two sets of simulations considering the cases of constant blood viscosity (Newtonian flow) versus radius-dependent viscosity (non-Newtonian flow) using the model proposed by Pries e. al. [21]. The model is derived from experimental data obtained at high shear rates ($\geq 50 s^{-1}$) and provides a clear correlation between blood viscosity in straight tubes, tube diameter and blood hematocrit.

Our findings indicate that the effect of non-Newtonian rheology is primarily manifested in the propagation of the pressure wave. In Figure 7 we present computed pressure waves using the *L/r* ansatz at the left internal carotid artery (CoW case, $r^* = 150\ \mu m$) and the axillary artery (arm case, $r^* = 500\ \mu m$). In both cases the fractal-trees are terminated at $r_{cut} = 20\ \mu m$, and the solutions have converged to a plateau where they are no longer sensitive to further decreasing the cut-off radius. We observe that modeling blood as a Newtonian uid has a signi cant effect on pressure wave propagation, resulting to an effective stiffening of the arterial wall response that leads to an upward shift of the pressure wave, pushing the predicted values away from the physiological range. On the other hand, the radius-depended viscosity model returned a physiologically correct solution, highlighting the fact that capturing non-Newtonian blood behavior is crucial for correctly modeling hemodynamics in small arteries and arterioles. Our results highlight that different rheology models may result to significantly different predictions far upstream in the network due to the cumulative effect of the large arteriolar networks modeled by the fractal tree.

3.4 Effect of distal outflow boundary conditions

The generated fractal arterial networks typically contain tens of thousands of distal outlets for which we need to provide a proper out flow boundary condition. Here, we demonstrate that the choice of the prescribed out flow boundary condition has minor effects on the predicted hemodynamics. To this end, we have considered three different types: absorbing wave, constant pressure, and 3-element windkessel boundary conditions. Absorbing conditions are applied by zeroing out the incoming Riemann invariant at the out flow boundary interface, ensuring that no wave reflections will occur. The use of constant pressure boundary conditions is primarily motivated by the fact that the pulsatility of the flow fades out as we approach the capillary bed (arterioles with radius $r < 30\ \mu m$), and estimates for the pressure values at these locations do exist in the medical literature [17]. Another possibility is to use simple 3-element windkessel models, consisting of a resistor in parallel with a resistor and capacitor (RCR), with the RCR parameters being roughly estimated based the total resistance of the constructed network and the target pressure values

at the outlet [1]. Note that due to very small variation of flowrate at terminals of the fractal network the RCR models becomes effectively the resistance model, i.e., the pressure-flowrate relation can be accurately estimated from $P = R_{total}Q$.

In Figure 8 we present the computed flowrate and pressure waveforms at representative locations for the CoW and arm networks. In both cases we have used the suggested L/r ansatz (CoW: $r^* = 150\ \mu m$, arm: $r^* = 500\ \mu m$), with the fractal-trees being terminated at $r_{cut} = 30\ \mu m$. The target pressure for the constant pressure and 3-element windkessel boundary conditions was set to 20mmHg, a representative value for small arterioles [17]. Our results indicate that both the mass flow distribution as well as the local pressure waves converge to a periodic state after two cardiac cycles (starting from zero-flow initial conditions) and show very low sensitivity to the choice of distal out flow boundary conditions. This observation advocates one of the key advantages of the proposed closure model as it seems to effectively eliminate uncertainties in out flow boundary conditions for hemodynamics.

4 Discussion

We have proposed an out flow closure model for blood flow simulations in large arterial networks, with our main goal being to obtain physiological flow predictions while reducing parametric sensitivities and circumventing costly calibration procedures. The model is based on resolving flow in self-similar networks of millions of small arteries and arterioles that are attached on-the-fly to a given parent vascular network of larger systemic arteries. To our knowledge, this is the first time that nonlinear 1D blood flow simulations have been performed in arterial networks of this size.

While the proposed model minimizes the overall time to accurate solution, it requires facilitation of parallel computers and a scalable solver. At the same time the number of processors (CPU cores) required for reasonable time-to-solution is still very low (less than 1000).This contribution is vital as, not only it allowed simulating trees with hundreds of thousand of arteries in the present work, but it opens the path to addressing many interesting open questions in computational hemodynamics. For instance, the proposed computational framework may be combined with flow and pressure measurements towards solving inverse problems (such as estimating material properties of the arterial wall, estimating the total volume of an arterial tree, etc).

We have suggested a way of addressing cut-off radius sensitivities by introducing a radius-dependent length-to-radius ratio for small arterioles, controlled by a threshold parameter, r^*. This ansatz led to flow predictions that gradually converge to a plateau solution as the cutoff radius is decreased, overcoming cutoff radius sensitivities previously reported for the structured tree out flow boundary condition [5].

Our proposed fractal closure model was thoroughly tested for two realistic cases of blood flow in the Circle of Willis and a detailed network of the arm vasculature. For the CoW case, where the parent network is patient-specific and the fractal model parameters are set according to a target volume estimate, the proposed model returns physiologically correct results without any user intervention or prior calibration. The key point here is that the

volume constraint can be achieved without performing any simulation based optimization (as opposed to tuning to match imposed/measured data), leading to significant savings in computation. Moreover, the volume constraint ts well the spirit of the structured tree as it has a physiological basis and enables the study of cases where having a physiologically correct tree is very important (for e.g. heterogeneous autoregulation).

For the arm case, the parent arm network is not-patient specific and a number of outlets may be missing. Moreover, a target volume estimate cannot be readily extracted from the literature, hence the threshold parameter r^* needs to be tuned. The main advantage of tuning r^* versus merely tuning a constant L/r ratio, is that the resulting model exhibits very low sensitivity on the cut-off radius r_{cut} as well as on the out flow boundary conditions used. The important lesson we learned here is that, in the absence of estimates for arterial blood volume in the truncated network, the convergence of flow and pressure waveforms with respect to the cut-off radius can still be obtained.

One limitation of the proposed method is the potential sensitivity on r^* for cases where a target volume estimate is not available. Although this introduces the need for calibration of r^*, we believe that the proposed framework is still viable as it only requires tuning of a single parameter, in contrast to tuning hundreds of resistance and capacitance parameters needed for the RCR model. Another practical limitation of the suggested methodology stems from the computational cost of solving the nonlinear flow equations in networks with hundreds of thousands of arteries. Such computations can be currently performed in a reasonable time only by utilizing computer clusters with a few hundreds of modern CPUs.

An immediate goal arising from this study is to apply the developed closure model for three-dimensional simulations of a blood flow in compliant arteries. That requires developing stable interface condition between the 3D and the 1D solvers and efficient coupling of the two parallel solvers. Another future thrust is to leverage on the robustness and scalability of the developed solver to address open problems in biomedicine, such as constructing global circulation models, performing high dimensional uncertainty quantification studies, as well as parameter estimation in inverse problems.

Acknowledgements

This work received partial support by the Air Force Offce of Scientific Research under Grant No. FA9550-12-1-0463, and the National Institutes of Health under Grant No. 1U01HL116323-01. We also thank Dr. Pablo J. Blanco, LLNC, Brazil, for providing the arm arterial model. Large scale computations have utilized resources at the Argonne Leadership Computing Facility at Argonne National Laboratory, through support by the DOE/INCITE program.

References

1. Alastruey J, Parker KH, Peiró J, Sherwin SJ. Lumped parameter outflow models for 1D blood flow simulations: effect on pulse waves and parameter estimation. Commun. Comput. Phys. 2008; 4:317–336.
2. Blanco PJ, Watanabe SM, Feijóo RA. Identification of vascular territory resistances in one-dimensional hemodynamics simulations. J. Biomech. 2012; 45:2066–2073. [PubMed: 22771032]
3. Cassot F, Lauwers F, Lorthois S, Puwanarajah P, Cances-Lauwers V, Duvernoy H. Branching patterns for arterioles and venules of the human cerebral cortex. Brain Res. 2010; 1313:62–78. [PubMed: 20005216]

4. Cousins, W. Ph.D. thesis. North Carolina State University; 2013. Boundary Conditions and Uncertainty Quantification for Hemodynamics..
5. Cousins W, Gremaud PA. Boundary conditions for hemodynamics: The structured tree revisited. J. Comput. Phys. 2012; 231:6086–6096.
6. Cousins W, Gremaud PA, Tartakovsky DM. A new physiological boundary condition for hemodynamics. SIAM J. Appl. Math. 2013; 73:1203–1223.
7. Craiem DO, Rojo FJ, Atienza JM, Armentano RL, Guinea GV. Fractional-order viscoelasticity applied to describe uniaxial stress relaxation of human arteries. Phys. Med. Biol. 2008; 53:4543. [PubMed: 18677037]
8. Doehring, TC.; Freed, AD.; Carew, EO.; Vesely, I., et al. J. Biomech. Eng.-T. Vol. 127. ASME; 2005. Fractional order viscoelasticity of the aortic valve cusp: an alternative to quasilinear viscoelasticity.; p. 700
9. Formaggia, L.; Quarteroni, A.; Veneziani, A. Cardiovascular Mathematics: Modeling and simulation of the circulatory system. Vol. 1. Springer Verlag; 2009.
10. Fung, Y. Biomechanics: Mechanical Properties of Living Tissues. Springer-Verlag; 1993.
11. Grinberg L, Cheever E, Anor T, Madsen JR, Karniadakis GE. Modeling blood ow circulation in intracranial arterial networks: a comparative 3D/1D simulation study. Ann. Biomed. Eng. 2011; 39:297–309. [PubMed: 20661645]
12. Grinberg L, Fedosov D, Karniadakis GE. Parallel multiscale simulations of a brain aneurysm. J. Comput. Phys. 2013; 244:131–147. [PubMed: 23734066]
13. Grinberg L, Karniadakis GE. Outflow boundary conditions for arterial networks with multiple outlets. Ann. Biomed. Eng. 2008; 36:1496–1514. [PubMed: 18612828]
14. Ito H, Kanno I, Iida H, Hatazawa J, Shimosegawa E, Tamura H, Okudera T. Arterial fraction of cerebral blood volume in humans measured by positron emission tomography. Ann. Nucl. Med. 2001; 15:111–116. [PubMed: 11448068]
15. Lombardi D. Inverse problems in 1D hemodynamics on systemic networks: A sequential approach. Int. J. Numer. Meth. Biomed. Engng. 2014; 30:160–179.
16. Mainardi, F. Fractional Calculus and Waves in Linear Viscoelasticity: An Introduction to Mathematical Models. Imperial College Press; 2010.
17. McDonald DA. Blood ow in arteries. 1974
18. Melani, A.; Quarteroni, A. Ph.D. thesis. EPFL; 2013. Adjoint-based parameter estimation in human vascular one dimensional models..
19. Olufsen MS. Structured tree outflow condition for blood flow in larger systemic arteries. Am. J. Physiol.- Heart C. 1999; 276:H257–268.
20. Perdikaris P, Karniadakis GE. Fractional-order viscoelasticity in one-dimensional blood flow models. Ann. Biomed. Eng. 2014; 42:1012–1023. [PubMed: 24414838]
21. Pries AR, Neuhaus D, Gaehtgens P, et al. Blood vicosity in tube flow: dependence on diameter and hematocrit. Am. J. Physiol. 1992; 263:H1770–H1770. [PubMed: 1481902]
22. Rengachary, SS.; Ellenbogen, RG. Principles of neurosurgery. Elsevier Mosby; 2005.
23. Reymond P, Bohraus Y, Perren F, Lazeyras F, Stergiopulos N. Validation of a patient-specific one-dimensional model of the systemic arterial tree. Am. J. Physiol.-Heart C. 2011; 301:1173–1182.
24. Sherwin SJ, Franke V, Peiro J, Parker KH. One-dimensional modelling of a vascular network in space-time variables. J. Eng. Math. 2003; 47:217–250.
25. Steele BN, Olufsen MS, Taylor CA. Fractal network model for simulating abdominal and lower extremity blood flow during resting and exercise conditions. Comput. Methods Biomech. Biomed. Engin. 2007; 10:39–51. [PubMed: 18651270]
26. VanBavel E, Spaan JA. Branching patterns in the porcine coronary arterial tree. estimation of flow heterogeneity. Circ. Res. 1992; 71:1200–1212. [PubMed: 1394880]
27. Watanabe SM, Blanco PJ, Feijóo RA. Mathematical model of blood flow in an anatomically detailed arterial network of the arm. ESAIM, Math. Model. Numer. Anal. 2013; 47:961–985.
28. Xiao N, Humphrey JD, Figueroa CA. Multi-scale computational model of three-dimensional hemodynamics within a deformable full-body arterial network. J. Comput. Phys. 2013; 244:22–40. [PubMed: 23729840]

29. Zamir M, et al. On fractal properties of arterial trees. J. Theor. Biol. 1999; 197:517–526. [PubMed: 10196094]

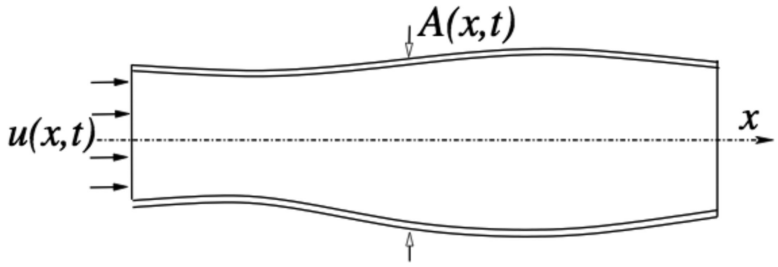

Figure 1.
Flow in a 1D compliant artery (from [24]).

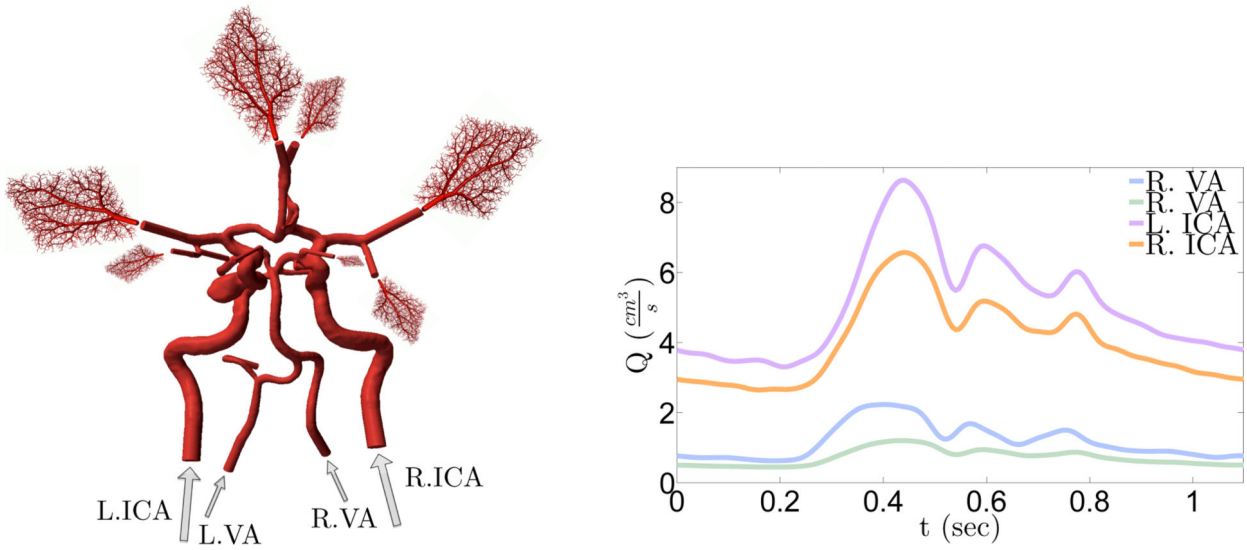

Figure 2.

Left: Fractal-trees are attached at each outlet of a parent patient-specific arterial network, resulting in an arterial domain with millions of compliant vessels in which blood flow is modeled using Eq. 1. The 1D parent network is constructed from the centerlines of the 3D geometry. *Right*: Flow is driven by high resolution, patient-specific PC-MRI measurements at the inlets (right vertebral artery R. VA, left vertebral artery L. VA, right internal carotid artery R. ICA and left internal carotid artery L. ICA).

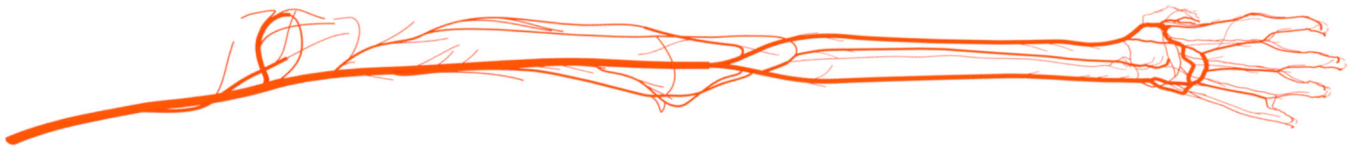

Figure 3.

A detailed arterial network of the arm, courtesy of Pablo J. Blanco, LLNC [27] (276 arteries with 105 terminal outlets, 124 bifurcation points, 18 merging junctions and 85 perforator vessels). The 1D parent network is constructed from the centerlines of the 3D geometry, while fractal trees are attached to each one of the 103 outlets.

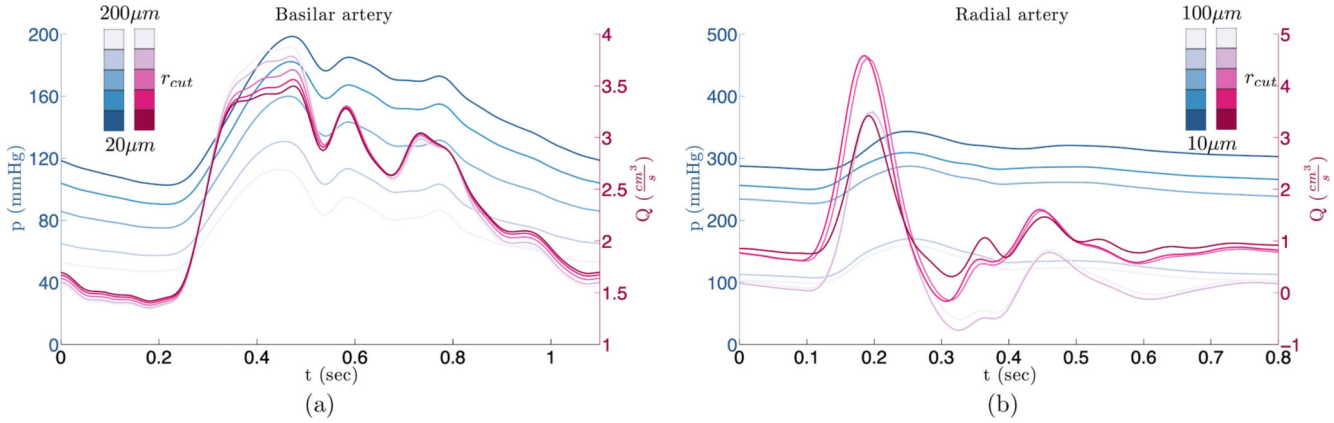

Figure 4.

Sensitivity on the cut-off radius r_{cut}: Computed pressure (*blue*) and flowrate (*red*) waves for different values of the cut-off radius r_{cut}, ranging from 200 to 10 μm. *Left*: Midpoint of the basilar artery (CoW case). *Right*: Midpoint of the radial artery (arm case).

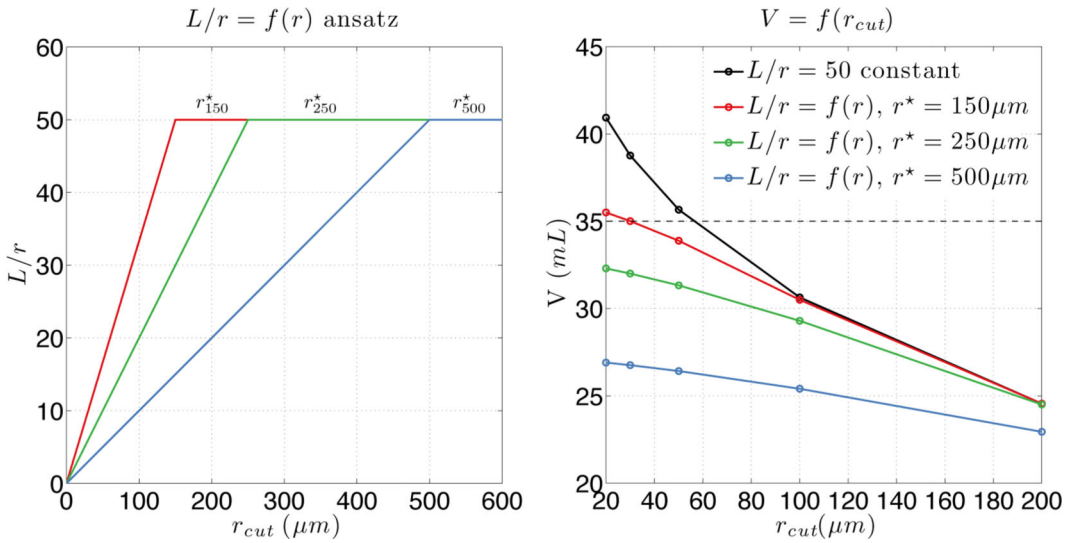

Figure 5.

Left: Decreasing *L/r* ansatz for different thresholds *r**. *Right*: Volume of the generated arterial tree as a function of the cut-off radius for different *L/r* relations (CoW case). The dashed line corresponds to the estimated target volume of 35*mL*.

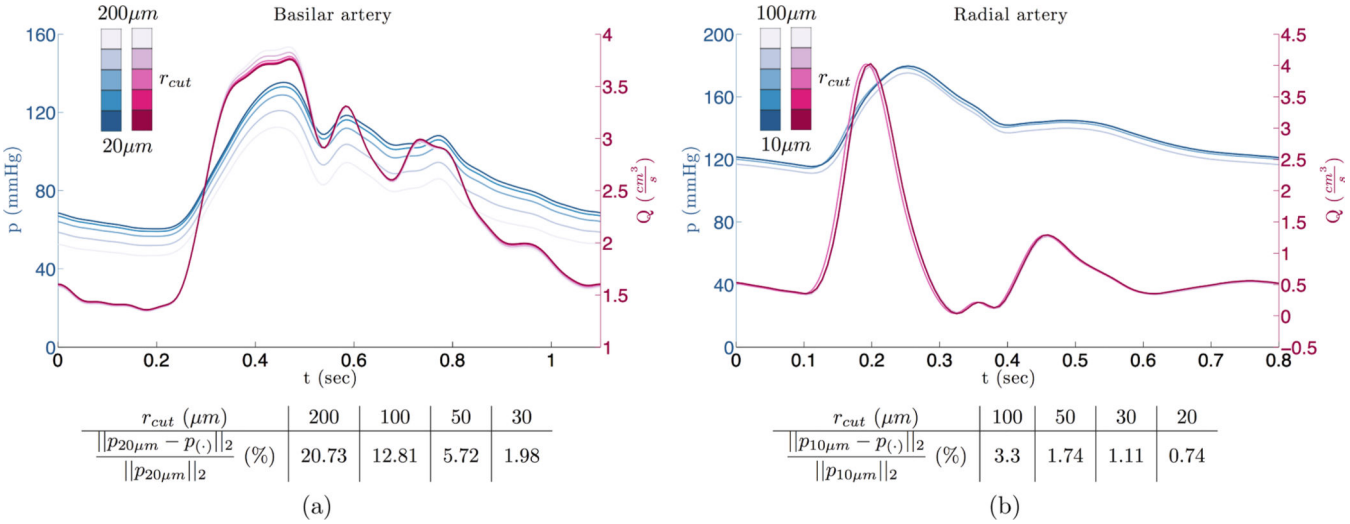

r_{cut} (μm)		200	100	50	30
$\frac{\|\|p_{20\mu m} - p_{(\cdot)}\|\|_2}{\|\|p_{20\mu m}\|\|_2}$	(%)	20.73	12.81	5.72	1.98

(a)

r_{cut} (μm)		100	50	30	20
$\frac{\|\|p_{10\mu m} - p_{(\cdot)}\|\|_2}{\|\|p_{10\mu m}\|\|_2}$	(%)	3.3	1.74	1.11	0.74

(b)

Figure 6.

Waveform convergence with decreasing cut-off radius using the *L/r* ansatz : Computed pressure (*blue*) and flowrate (*red*) waves for different values of the cut-off radius r_{cut}. *Left*: Midpoint of the basilar artery (CoW case). *Right*: Midpoint of the radial artery (arm case). Inscribed tables contain the relative error (L_2 norm) of the pressure wave as we decrease the cut-off radius (reference cases: r_{cut} = 20 *μm* for CoW and r_{cut} = 10 *μm* for the arm).

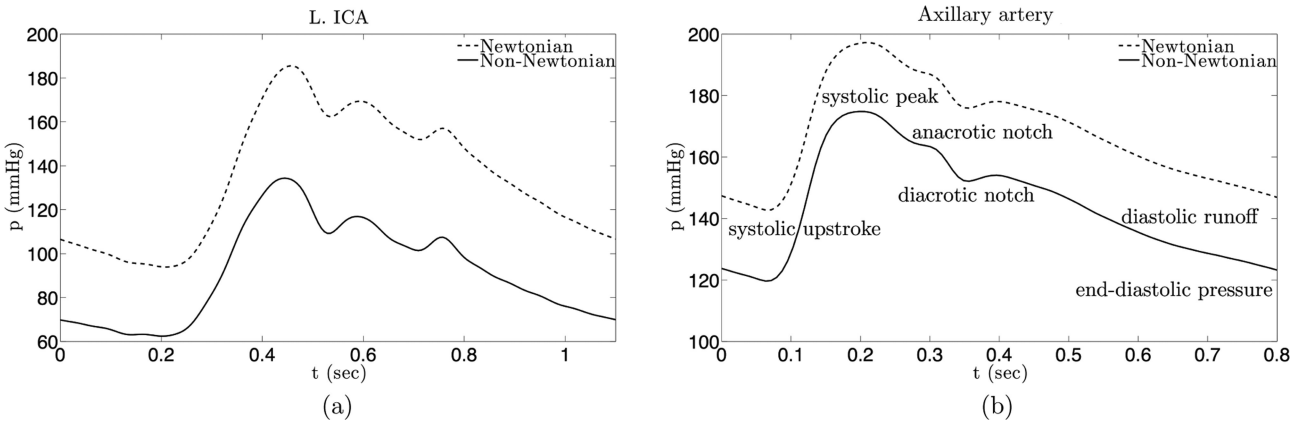

Figure 7.

Computed pressure waves for different blood rheology models: radius-depended viscosity [21] (non-Newtonian, *solid line*) versus constant blood viscosity (Newotnian, *dashed line*) *Left*: Inlet of the left internal carotid artery (L. ICA, CoW case). *Right*: Inlet of the axillary artery (arm case).

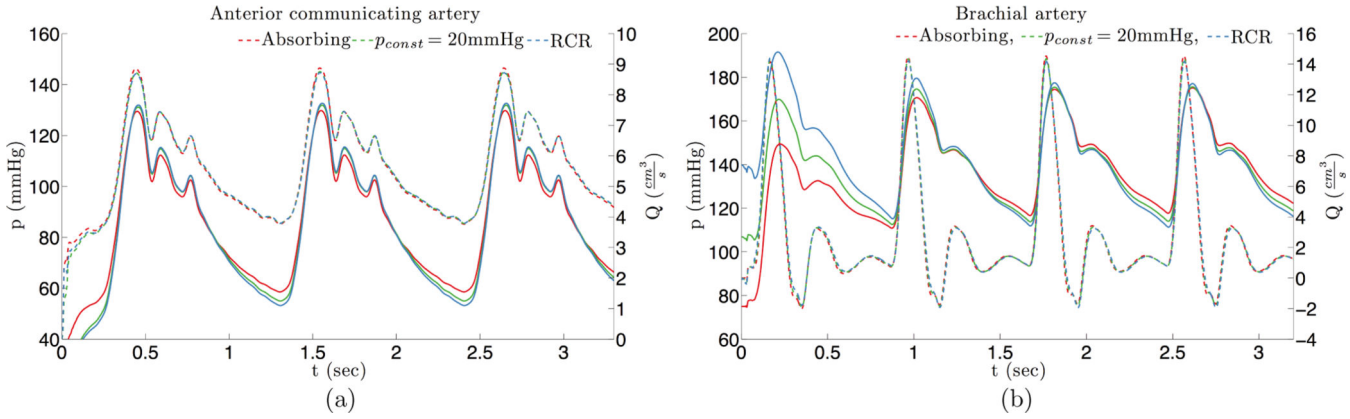

Figure 8.

Effect of distal outflow boundary conditions: Computed pressure (*solid lines*) and flowrate (*dashed lines*) waves for different types of distal outlfow boundary conditions: Absorbing (*red*), constant pressure (*green*), and 3-element RCR windksessels (*blue*). *Left*: Anterior communicating artery (AcoA, CoW case). *Right*: Brachial artery (arm case). Figure legends indicate the colors to which each outflow model corresponds to.

Table 1

Total number of vessels and average number of generations attached to each outlet of the parent CoW and arm networks as a function of the fractal-tree cut-off radius r_{cut}. The average number of generations is calculated by averaging over all terminal outlets of the parent network.

	CoW		Arm	
$r_{cut}(\mu m)$	No. of vessels	Avg. No. of gen.	No. of vessels	Avg. No. of gen.
200	1,286	14	-	-
100	8,456	21	1,400	14
50	56,484	27	9,046	19
30	226,522	32	36,228	24
20	682,450	36	109,567	28
10	4,392,484	43	702,188	34